Available online at www.sciencedirect.com
ScienceDirect
Ceramics International 37 (2011) 2537–2541
CERAMICS INTERNATIONAL
www.elsevier.com/locate/ceramint

An efficient way to improve the electrical stability of $Ni_{0.6}Si_{0.2}Al_{0.6}Mn_{1.6}O_4$ NTC thermistor

Sen Liang *, Jianfeng Yang, Xiaohong Yi, Xiao Zhang, Yu Bai

The Sate Key Laboratory for Mechanical Behavior of Materials, Xi'an Jiaotong University, Xi'an 710049, China

Received 13 January 2011; received in revised form 25 March 2011; accepted 31 March 2011
Available online 8 April 2011

Abstract

In this paper, $Ni_{0.6}Si_{0.2}Al_{0.6}Mn_{1.6}O_4$ compounds with negative temperature coefficient (NTC) property were fabricated using NiO, SiO_2, MnO_2 and Al_2O_3 as raw materials. The effect of ball milling time on phase composition, microstructure and electrical stability of the compounds was studied. The results showed that the particle size of calcined powder decreased with the increase of ball-milling time, resulting in a decreased $B_{25/85}$ constant, activation energy and resistance drift $\Delta R/R_0$ (%) of the $Ni_{0.6}Si_{0.2}Al_{0.6}Mn_{1.6}O_4$ compounds. Meanwhile, it was found that activation energy increased with the decrease of the density of the compounds, and the resistance drift $\Delta R/R_0$ (%) was less than 0.02% when the ball-milling time reached to 48 h.

Keywords: C. Electrical properties; NTC; Aging; Ball-milling

1. Introduction

Ascribing to the smart property that the resistance decreases with increasing temperature, negative temperature coefficient thermistor (NTC) is considered as one of the high performance ceramic materials and has been used in fabricating temperature sensors [1,2]. Electrical properties of the NTC thermistors after a long-term exposure at elevated temperatures, i.e. 150 °C was stable [3]. However, the main problem of these materials is aging, which refers to a drift of the resistivity with time (500–1000 h). The aging often occurs during using of the thermistors at elevated temperatures (i.e. 150 °C) [4]. In general, NTC thermistors are spinel-like ceramics with the formula of AB_2O_4, which are based on the mixed oxides of Mn, Ni, Fe, Co and Cu [5,6]. In the spinel structure, two sites are available for the cations: the tetrahedral site (A-site) and octahedral site (B-site). It is generally accepted that the exchange of cations between sublattice tetrahedral (A-sites) and octahedral (B-sites) result in the aging of Fe-containing NTC thermistors [4,7–13]. Besides, some studies showed that the aging also involves migration of cation vacancies from the grain boundaries to the interior [14].

The typical NTC thermistor preparation method was conventional solid-state synthesis processing, the screen printing and electron-beam evaporation (EBE) technology were also used to fabricate film NTC thermistor [15–19]. The physical properties of NTC thermistors depend on the preparation technique and the particle morphology [9]. Hosseini and Yasaei reported that the electrical resistivity decreased with increasing grain size, and attainment of high density microstructure controlled by grain size and appropriate dimensional designs was the key factor in fabricating high-performance sensor [20]. So, in the present study, one novel and efficient approach to improve the electrical properties of $Ni_{0.6}Si_{0.2}Al_{0.6}Mn_{1.6}O_4$ NTC materials is addressed. And the effect of ball-milling time on the microstructure and electrical properties of the $Ni_{0.6}Si_{0.2}Al_{0.6}Mn_{1.6}O_4$ NTC materials was studied in details.

2. Experimental

High-purity (analytical grade) NiO, SiO_2, MnO_2 and Al_2O_3 powders (Sinopharm Chemical Reagent Co. Ltd., China) were weighed respectively according to the stoichiometric composition of $Ni_{0.6}Si_{0.2}Al_{0.6}Mn_{1.6}O_4$. The weighed powders and

* Corresponding author at: Sate Key Laboratory for Mechanical Behavior of Materials, Xi'an Jiaotong University, No. 28, Xianning West Road, Xi'an, Shaanxi 710049, China. Tel.: +86 29 82667942 803; fax: +86 29 82667942 804.
E-mail addresses: yang155@mail.xjtu.edu.cn, lsen110@gmail.com (S. Liang).

0272-8842/$36.00
doi:10.1016/j.ceramint.2011.03.061

alcohol were mixed and milled for 12 h in a plastic jar using agate balls as grinding media. The obtained slurry was dried at 80 °C in an oven for 12 h, following by calcination in alumina crucible at 950 °C for 2 h. The mixture was further milled for 6 h, 12 h, 24 h, and 48 h, respectively. The dried powders were ground in mortar and passed through a 200-mesh sieve. Polyvinyl alcohol (PVA) solution (PVA/distilled water = 5:95 in weight) was added into the powders and the mixtures were ground in mortar, followed by ball-milled for 2 h in plastic jar using agate balls. The mixture powders were uniaxially pressed at the pressure of 180 MPa and the cylindrical pellets with diameter of 10 mm and thickness of 5 mm were obtained. The green compacts were heated in air from room temperature to 500 °C at the heating rate of 20 °C/h to remove the organic binder, and then were sintered at 1280 °C for 4 h in the ambient air furnace, followed by a natural cooling. In order to measure the resistances, the high temperature Ag pastes were applied on two-sides of the sintered samples. After drying of the pastes, the samples were heated at 750 °C for 20 min.

The particle size of powders was measured using by laser particle size analyzer (Rise-2008, Jinan, China). The phase and crystalline structure of the samples were characterized by X-ray diffraction (XRD) using Cu Kα radiation (Rigaku X-Ray Diffractometer, Japan). The microstructures of samples were investigated using a scanning electron microscope (SEM) (VEGAII XMU, Tescan, Czech Republic). Electrical measurements of resistance vs. temperature were performed using digital measurements (Fluke8846, U.S.A.). The thermistor constant B was calculated according to Eq. (1):

$$B = \frac{(\ln R_1 - \ln R_2)}{(1/T_1) - (1/T_2)} \quad (1)$$

R_1 and R_2 are the resistances at temperatures T_1 and T_2, respectively. The relative 25 °C resistance change, $\Delta R/R$ (%), of the samples is defined by the following Eq. (2):

$$\frac{\Delta R}{R_0}(\%) = \frac{R_1 - R_0}{R_0} \times 100 \quad (2)$$

where R_0 is the resistivity at 25 °C for the initial test, and R_1 is the resistivity at 25 °C after soaking these samples in an oven at 150 °C for 500 h.

3. Results and discussion

3.1. Particle size distribution

The results obtained from laser particle size analyzer revealed that the average median particle size (D_{50}) for the original powders of NiO, MnO_2, SiO_2 and Al_2O_3 were 1.2, 60.3, 17.2, 23.4 μm, respectively, which indicated that the original powders covered a wide range of particle size. Fig. 1 shows the particle size distributions of powders after calcined at 950 °C for 2 h and then ball-milled for 6 h, 12 h, 24 h and 48 h, respectively. As shown in Fig. 1, the powders ball-milled for 24 h and 48 h exhibited a narrower particle size distribution, as compared with the powders ball-milled for 6 h and 12 h. In addition, the powders

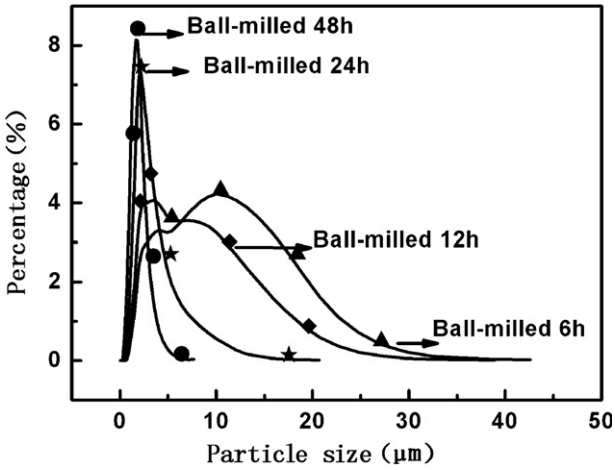

Fig. 1. Comparison of particle size distribution curves of different ball-milling times.

ball-milled for 6 h and 12 h exhibited a bimodal distribution, and only narrow peak was observed when the ball-milling time reached to 24 or 48 h. The D_{50} for ball-milling for 6 h, 12 h, 24 h and 48 h were 6.1, 4.1, 2.2, 1.5 μm, respectively. The above results indicated that the particle size of calcined powders decreased with the extension of ball-milling time.

3.2. X-ray diffraction analysis

The samples using the powders obtained by ball milling for 6 h, 12 h, 24 and 48 h were marked as I, II, III and IV, respectively.

Fig. 2 shows the XRD analysis of samples after sintered at 1280 °C in air for 4 h. As seen from it, the samples I, II and III had the same XRD patterns, which were composed of cubic spinel and Al_2O_3 phases. However, the Al_2O_3 phase was scarcely recognized in the sample IV. The Al_2O_3 phase in samples I, II and III was originated from the starting powders, and its content was decreased with ball-milling time increased.

For the purpose of detecting if any cubic spinel Ni-rich phase was present in spinel, as suggested by Park et al. [21], the 2θ ranged from 55° to 64° was set to give a distinguishing of them.

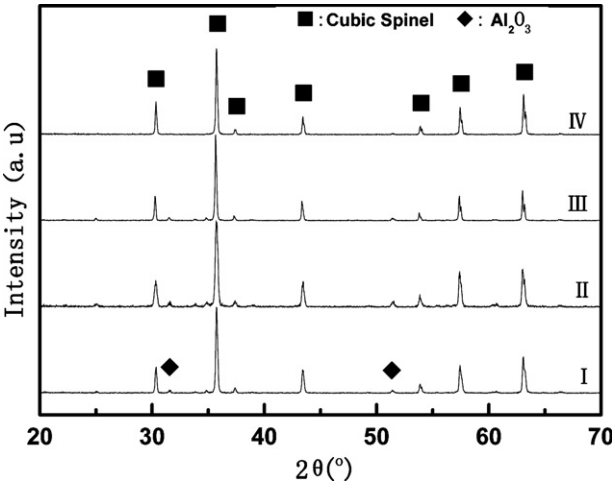

Fig. 2. XRD patterns of $Ni_{0.6}Si_{0.2}Al_{0.6}Mn_{1.6}O_4$ ceramic sintered at 1280 °C in air.

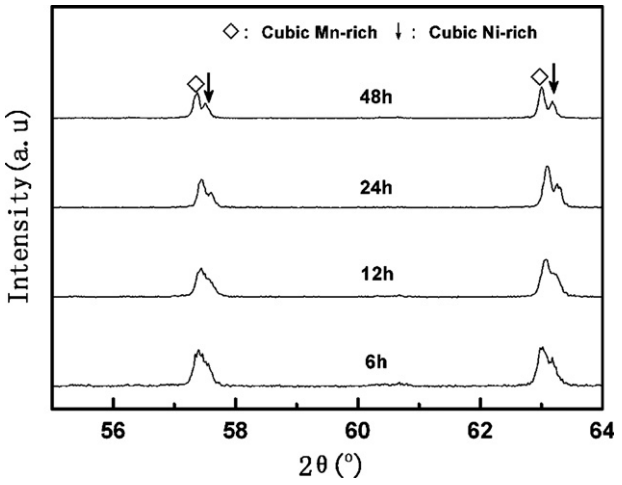

Fig. 3. Selected XRD patterns of $Ni_{0.6}Si_{0.2}Al_{0.6}Mn_{1.6}O_4$ ceramic sintered at 1280 °C in air.

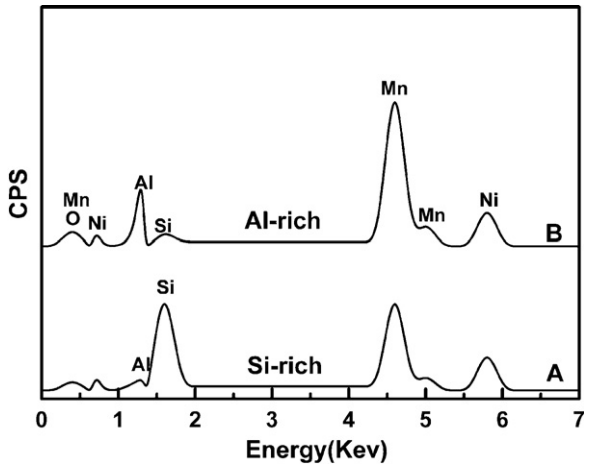

Fig. 5. EDS spectra of the area marked with "A" and "B".

The XRD patterns are shown in Fig. 3, and it was found that the cubic spinel phase was composed of two phases: a major Mn-rich phase and Ni-rich phase. So, it can be concluded that three phases coexisted in the sintered samples, namely cubic Mn-rich spinel phase, cubic Ni-rich spinel phase and Al_2O_3 phase.

3.3. SEM analysis

Fig. 4 illustrates the SEM images of the as-sintered samples. All the samples showed a homogeneous microstructure, and the density of samples reached to 78, 82, 92, 99% of the theoretical density, respectively. It indicated that the density increased with the decrease of particle size of raw calcined powder due to the high sintering activity.

From the SEM image of sintered samples, the grain size was similar, ranging from 2 to 10 μm. In addition, two kinds of grain morphology in the sintered bodies were found, which were marked by "A" and "B" in Fig. 4. The EDS was used to investigate the chemical composition and the results are shown in Fig. 5 for the two kinds of grain morphology. The average concentrations of Ni, Mn, Si and Al in the area A were 24, 36, 27 and 1 at.%, respectively, while that in area B were 18, 46, 5 and 16 at.%, respectively. Compared to the nominal composition of the ceramic ($Ni_{0.6}Si_{0.2}Al_{0.6}Mn_{1.6}O_4$), the A area was rich in the Si and Ni, which was identified as Ni-rich phase or

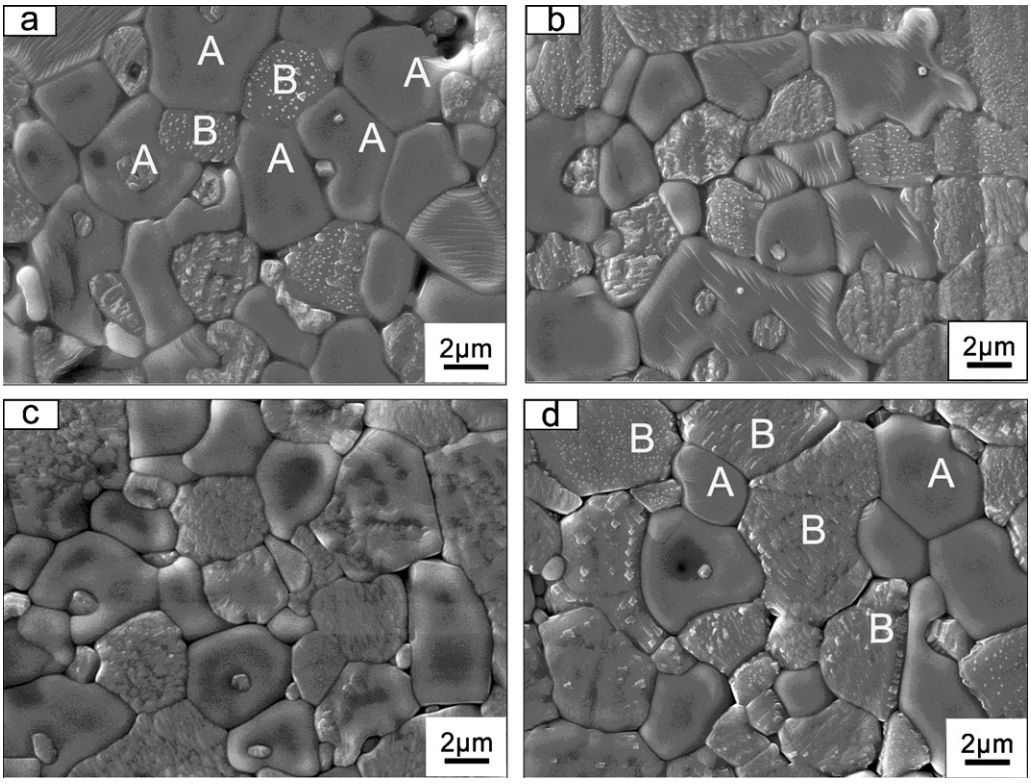

Fig. 4. SEM micrographs of the as-sintered samples (a) I; (b) II; (c) III; (d) IV.

Si-rich phase, while the ''B'' area was done as Mn-rich phase. The above results also suggested that Al had a priority to react with Mn as compared with Ni, whereas Si was easier to react with Ni than Mn. In addition, it was found that the Ni-rich (Si-rich phase) phase showed a smooth structure, whereas the Mn-rich phase showed a coarse structure. Park et al. named this structure as twin-containing [21]. A software (Image-Pro Plus) was used to quantify the concentration of two different phases. The results showed that the average area concentrations of the Ni-rich phase were 50.54, 65.27, 47.63, 31.49%, and those of the Mn-rich phase were 49.46, 34.73, 52.37, 68.51% for the samples I, II, III and IV, respectively.

3.4. Electrical measurement

It was found that the electrical resistivity (ρ) of the $Ni_{0.6}Si_{0.2}Al_{0.6}Mn_{1.6}O_4$ NTC thermistors decreased with the increase of temperature. The logarithm of the electrical resistivity, ln ρ, as a function of the reciprocal of the absolute temperature, 1/T, with four kinds of samples is shown in Fig. 6. All thermistors showed a linear relationship for the ln ρ with 1/T in the measured temperature range (room temperature ~300 °C), indicating the good agreement of NTC thermistor characteristics as described by the Nernst–Einstein relation [22]. The conductivity mechanism of nickel manganite spinel materials was explained by many researchers [7,12,13,23], and they considered that the conductivity depended on the change in concentration and ordering of hopping charge carriers namely Mn^{3+} and Mn^{4+} at octahedral site.

Table 1 gives the ρ_{25}, $B_{25/85}$ constant, activation energy and resistance drift (aging), which are the most important characteristics of technical interest for NTC thermistors. The resistivity of four kinds of samples at room temperature showed an interesting tendency, with the increase of ball-milling time, it decreased when the milling time was less than 12 h, and then dramatically increased up to 48 h. The minimum value of resistivity was measured from the sample II which was ball-milled for 12 h. The resistivity of the materials depends on several factors, such as phase and structure. From the above SEM results (Fig. 4), the content of Ni-rich phase was 50.54, 65.27, 47.63, 31.49% for the four kinds of samples, respectively; and one interesting phenomenon was that the samples showed an inverse relationship between the content of Ni-rich phase and the resistivity at room temperature. The relation between the content of Ni-rich phase and resistivity can be explained as follows: the content of Mn-rich phase was increased with decreasing Ni-rich phase (Fig. 4) and the Al had a priority to react with Mn in compared with Ni (Fig. 5). So the content of Al also increased with decreasing Ni-rich phase. In the spinel, O^{2-} ions form a cubic close-packed array, and Al^{3+} ions had a preference for occupying the octahedral sites according to the crystal field theory, so with the increase of Al content, the number of the Mn^{3+}/Mn^{4+} couples for hopping was decreased, resulting in increased resistivity.

Table 1
Resistivity at room temperature, $B_{25/85}$, activation energy and resistance drift (aging) for four kinds of NTC thermistors samples.

Sample	ρ (25) (Ω cm)	$B_{25/85}$ constant (K)	Activation energy (eV)	Resistance drift (%)
I	8.06×10^6	5166	0.4456	6.02
II	6.57×10^6	4952	0.4271	4.87
III	1.02×10^7	4876	0.4206	1.82
IV	1.36×10^7	4817	0.4155	0.02

Previous study has shown the activation energy (ΔE) dependence of the porosity for ionic conductivity ceramic material [24]. In the same way, the increase of the activation energies with the density is presented in Fig. 7. Porosity and density were two conflicting parameters, and the porosity decreased with the increase of density. As shown in Fig. 7, it was found that the activation energy decreased with the increase of density. Meanwhile, this tend also indicated that higher activation energy was required for a material with higher porosity.

From the results of resistance drift ($\Delta R/R_0$) as shown in Table 1, it decreased with the increase of ball-milling time. A resistance drifts of less than 0.02% was obtained for the sample IV, which was ball-milled for 48 h. The aging phenomenon

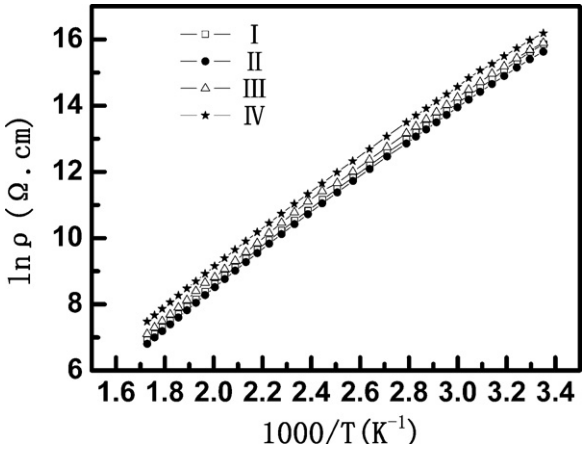

Fig. 6. Plot of ln ρ vs. reciprocal of temperature for four kinds of thermistor samples.

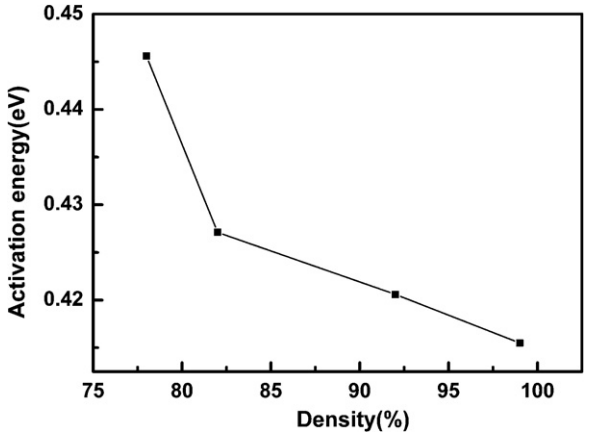

Fig. 7. Activation energy dependence of density of $Ni_{0.6}Si_{0.2}Al_{0.6}Mn_{1.6}O_4$ NTC thermistors.

could be explained by the contact degradation [25] and cationic migration [4]. The resistance drift of less than the 0.02% indicated excellent reliability of the $Ni_{0.6}Si_{0.2}Al_{0.6}Mn_{1.6}O_4$ NTC thermistor. By the ball-milling with proper time (i.e. 24 h to 48 h), well-refined powder could be obtained, and the electricity reliability of NTC thermistor could also be improved through sintering these powders.

4. Conclusion

The high stable $Ni_{0.6}Si_{0.2}Al_{0.6}Mn_{1.6}O_4$ NTC thermistors with different electrical properties were fabricated through proper ball-milling of calcined powders, by tailoring the phase composition and the microstructure. The $B_{25/85}$ constant, activation energy and resistance drift $\Delta R/R_0$ (%) decreased with the increase of ball-milling time. Furthermore, the resistance drift $\Delta R/R_0$ (%) of less than the 0.02% was obtained for the sample of ball-milling for 48 h.

Acknowledgments

This work was supported by the National Natural Science Foundation of China (Grant Nos. 51072157, 50821140308), and by Doctoral Fund of Ministry of Education of China (Grant No. 20100201110036). And thank Mr. Yunguo Yu for writing assistance.

References

[1] J.W. Zhuang, et al., The effects of pH value on the characterization of CoMnNiO NTC thermistor nanopowders, Ceram. Int. 30 (2004) 1661–1663.
[2] C. Zhao, et al., Effects of Cu and Zn co-doping on the electrical properties of $Ni_{0.5}Mn_{2.5}O_4$ NTC ceramics, J. Eur. Ceram. Soc. 28 (2008) p35.
[3] M. Vakiv, et al., Ageing behavior of electrical resistance in manganite NTC ceramics, J. Eur. Ceram. Soc. 24 (2004) 1243–1246.
[4] W.A. Groen, et al., Aging of NTC ceramics in the system Mn–Ni–Fe–O, J. Eur. Ceram. Soc. 21 (2001) 1793–1796.
[5] A. Veres, et al., Manganese based spinel-like ceramics with NTC-type thermistor behaviour, Solid State Ionics 178 (2007) 423–428.
[6] K. Park, et al., Improvement in the electrical stability of Mn–Ni–Co–O NTC thermistors by substituting Cr_2O_3 for Co_3O_4, J. Alloy Compd. 437 (2007) 211–214.
[7] A. Feltz, P. Walter, Spinel forming ceramics of the system $Fe_xNi_yMn_{3-x-y}O_4$ for high temperature NTC thermistor applications, J. Eur. Ceram. Soc. 20 (2000) 2353–2366.
[8] S.A. Kanade, V. Puri, Properties of thick film $Ni_{0.6}Co_{0.4}Fe_yMn_{2-y}O_4$: $(0 \leq y \leq 0.5)$ NTC ceramic, J. Alloy Compd. 475 (2009) p.352–355.
[9] I.P. Muthuselvam, R.N. Bhowmik, Structural phase stability and magnetism in Co_2FeO_4 spinel oxide, Solid State Sci. 11 (2009) 719–725.
[10] K. Park, Structural and electrical properties of $FeMg_{0.7}Cr_{0.6}Co_{0.7-x}Al_xO_4$ $(0 \leq x \leq 0.3)$ thick film NTC thermistors, J Eur. Ceram. Soc. 26 (2006) 909–914.
[11] D. Saha, et al., Preparation of bixbyite phase $(Mn_xFe_{1-x})_2O_3$ for NTC thermistor applications, Mater. Lett. 55 (2002) 403–406.
[12] J.M. Varghese, A. Seema, K.R. Dayas, Microstructural, electrical and reliability aspects of chromium doped Ni–Mn–Fe–O NTC thermistor materials, Mater. Sci. Eng. B 149 (2008) 47–52.
[13] Z. Wang, et al., X-ray diffraction and infrared spectra studies of $Fe_xMn_{2.34-x}Ni_{0.66}O_4$ $(0 < x < 1)$ NTC ceramics, J. Eur. Ceram. Soc. 26 (2006) 2833–2837.
[14] Z. Wang, et al., Effect of annealing in O_2 or N_2 on the aging of $Fe_{0.5}Mn_{1.84}Ni_{0.66}O_4$ NTC-ceramics, Solid State Ionics 177 (2006) 2191–2194.
[15] M. Hrovat, et al., Thick-film NTC thermistors and LTCC materials: the dependence of the electrical and microstructural characteristics on the firing temperature, J. Eur. Ceram. Soc. 29 (2009) 3265–3271.
[16] J. Huang, et al., Preparation and characteristic of the thermistor materials in the thick-film integrated temperature-humidity sensor, Mater. Sci. Eng. B 99 (2003) 523–526.
[17] S. Jagtap, et al., Study of microstructure, impedance and dc electrical properties of RuO_2-spinel based screen printed 'green' NTC thermistor, Curr. Appl. Phys. 10 (2010) 1156–1163.
[18] P. Fau, et al., Thin films of nickel manganese oxide for NTC thermistor applications, Appl. Surf. Sci. 65–66 (1993) 319–324.
[19] M. Lee, M. Yoo, Detectivity of thin-film NTC thermal sensors, Sens. Actuators A 96 (2002) 97–104.
[20] M. Hosseini, B. Yasaei, Effect of grain size and microstructures on resistivity of Mn–Co–Ni thermistor, Int. Ceram. 24 (1998) 543–545.
[21] K. Park, et al., The effect of Zn on the microstructure and electrical properties of $Mn_{1.17-x}Ni_{0.93}Co_{0.9}Zn_xO_4$ $(0 \leq x \leq 0.075)$ NTC thermistors, J. Alloy Compd. 467 (2009) p.310–316.
[22] K. Park, J.K. Lee, Mn–Ni–Co–Cu–Zn–O NTC thermistors with high thermal stability for low resistance applications, Scripta Mater. 57 (2007) 329–332.
[23] G.D.C. Csete de Györgyfalva, I.M. Reaney, Decomposition of $NiMn_2O_4$ spinel: an NTC thermistor material, J. Eur. Ceram. Soc. 21 (2001) 2145–2148.
[24] P.J. Panteix, et al., Influence of porosity on the electrical properties of $La_{9.33}(SiO_4)_6O_2$ oxyapatite, Ceram. Int. 34 (2008) 1579–1586.
[25] J.M. Varghese, A Seema, K.R. Dayas, Microstructural, electrical and reliability aspects of chromium doped Ni–Mn–Fe–O NTC thermistor materials, Mater. Sci. Eng. B 149 (2008) 47–52.